energy&fuels

pubs.acs.org/EF

Article

New Nuclear Magnetic Resonance Approaches on the Evolution of Wax Mobility during Wax Crystallization

George Claudiu Savulescu,* Sébastien Simon, Geir Sørland, and Gisle Øye

Cite This: *Energy Fuels* 2022, 36, 350−360

Read Online

ACCESS | Metrics & More | Article Recommendations | Supporting Information

ABSTRACT: Wax crystallization at low temperature is one of the main problems affecting flow assurance during oil production. Wax inhibitors, such as pour point depressants (PPDs), and crude oil components, such as asphaltenes, are estimated to impact wax precipitation by both cocrystallization and the formation of complexes with waxes. However, the exact mechanism behind these interactions is not fully understood. Low field nuclear magnetic resonance (LF-NMR) methods have rarely been implemented for the analysis of wax precipitation in crude oil in spite of very promising results. This paper presents an improved method focused on the measurement of relaxation times which characterize the mobility of wax, asphaltene, and PPD molecules. As a wax crystal network forms at low temperature due to wax precipitation, dissolved wax molecules display a reduction in mobility as they become trapped in the pores and interact with the species of solids in the crystal network. The aim of this article is to analyze wax−wax and wax−inhibitor interactions by quantifying the amount of wax molecules trapped inside the crystal network. This paper focuses on investigating the effect of wax, asphaltene, and PPD concentrations on the percentage of precipitated wax with temperature and on the intensity of the reduced mobility wax region. The novelties of this work include the identification and quantification of a low mobility asphaltene nanoaggregate region, which may be used in future studies to characterize the changes in asphaltene aggregation state over selected concentration ranges. Additionally, the new NMR method allows us to understand and quantify with high resolution how asphaltenes in evolving aggregation states or other inhibitors impact the mobility of the dissolved wax within the wax crystal network. The new methods and breakthroughs about the wax precipitation mechanism may be correlated and extended in future studies to observations in real crude oil systems.

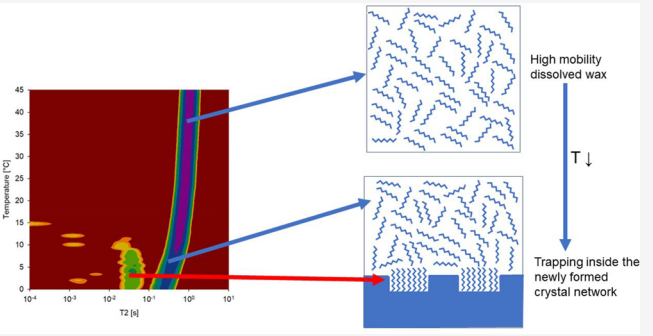

1. INTRODUCTION

Paraffin waxes are components of crude oil, consisting of *n*-, iso-, or cyclo-alkanes, usually with a carbon chain between C_{20} and C_{100} or even higher.[1] Wax precipitation occurs in a fluid environment at temperatures lower than the wax appearance temperature (WAT). This phenomenon negatively impacts flow assurance during crude oil extraction. Wax deposition during continuous flow pipeline restart issues caused by waxy gelling and increased fluid viscosity are among the problems most often encountered as a result of wax precipitation.[2]

Wax crystallization is expected to take place in three stages: nucleation, growth, and agglomeration. When temperature is gradually decreased, nucleation is delayed by a time lag, required to overcome the gap from steady-state conditions. This delay is dependent on the cooling rate,[3] and thus, the observed cloud point in such experiments is lower than the actual solubility point of wax. During the last phase of crystallization, a gel is usually formed in systems with a high enough wax content (at least 1%−2%).[4] The properties of the gel are dependent on several factors. including the wax composition. For example, macrocrystalline wax, usually composed of low molecular weight *n*-alkanes (C_{18}−C_{40}) with a more linear structure, is expected to manifest high yield strength gels, due to larger and less compact crystal structures. On the other hand, microcrystalline wax, composed of high molecular weight (C_{40} and above), iso-alkanes and cyclo-alkanes usually generate weak gels due to smaller and more compact crystal structures.[5]

A conventional method to combat wax-related issues is the use of wax inhibitors, such as pour point depressants (PPDs).[6] Although it was not completely demonstrated, the wide perception is that PPDs react with wax by cocrystallization and by affecting wax nucleation and solubility.[7] The presence of asphaltenes, polar components in crude oil, can also impact

Received: October 22, 2021
Revised: December 10, 2021
Published: December 23, 2021

wax precipitation. Asphaltenes represent high molecular compounds in crude oil, which are insoluble in low molecular weight *n*-alkanes but are soluble in aromatic solvents such as toluene.[8] In some cases, asphaltenes were found to cocrystallize with wax to smaller and distorted crystals, which creates significant improvements to crude oil flowability.[9] Also, asphaltenes can act as a nucleation site for wax, generating more finely dispersed wax crystals, which again allow better crude oil flow but might increase WAT.[9−12] However, the exact mechanism behind the impact of asphaltenes on wax precipitation remains to be further investigated. Previous studies often have contradicting conclusions. Some works show that asphaltenes inhibit wax precipitation in certain concentration regions, specific to each type of asphaltenes, but they might promote wax precipitation in other concentration regions.[13,14] The pattern of the concentration ranges for crystallization inhibition or promotion is in most cases rather irregular, mainly because of the polydisperse character of asphaltenes,[15] and remains to be investigated with higher accuracy. In addition to PPDs and asphaltenes, isomer waxes with more branched alkane composition (microcrystalline) present in relatively high concentrations (1 wt % microcrystalline, 5 wt % macrocrystalline wax system) have recently been investigated as a modifier to macrocrystalline wax crystallization patterns.[16] The microcrystalline waxes have been shown to prevent interlocking in macrocrystalline waxes through spatial hindrances. This phenomenon leads to the formation of only small and discrete macrocrystalline wax crystals, which make the system behave like a microcrystalline gel.[16]

Researchers in this field have so far studied the effects of wax inhibitors on wax deposition with analytical methods such as differential scanning calorimetry (DSC), cross-polarized microscopy (CPM), isothermal titration calorimetry (ITC), and more recently low field NMR.[2,17−21]

Batsberg Pedersen et al. first introduced low field NMR for the analysis of wax precipitation in crude oils.[22] They compared the amount of precipitated waxes and the amount of waxes determined by the acetone precipitation method for 17 crude oils. Throughout time, the procedure has been extensively developed and improved in accuracy.[23,24]

In recent years, an adapted Carr−Purcell−Meiboom−Gill (CPMG) sequence (see below) has been used to characterize crude oil systems. For example, Yalaoui et al.[25] investigated the behavior of the crude oil within the crystal network formed during crystallization and illustrated the presence of a region with lower mobility liquid trapped in the crystal network. However, these regions could not be entirely separated and quantified due to the strong proton signal generated by the other liquid components of the crude oil.

Zhao et al. adapted the CPMG sequence to characterize model wax systems in deuterated toluene in order to prevent this form of overlapping.[21] Wax precipitation curves, tracking the apparent solid content, were generated by quantifying the change in the dissolved wax signal in various wax and wax−PPD systems. Ruwoldt et al. extended the method to study the impact of a wider range of inhibitors on wax precipitation,[19] demonstrating the effectiveness and sensitivity of the method. Direct comparison of wax precipitation curves with DSC proved that the two methods generated consistent results.

This study aims to create a higher resolution NMR method which provides additional insight into the interactions behind the wax inhibition mechanism, such as complex formation between dissolved wax and particles in the newly formed crystal network and cocrystallization of wax and inhibitor molecules.

2. THEORY

2.1. Nuclear Magnetic Resonance (NMR). When placing a sample containing protons in an external field, the nuclear magnetic moment of the protons will align against this field. By applying for a short time an oscillating magnetic field with a frequency corresponding to the energy needed to induce transitions between the nuclear energy levels (the resonance frequency), the system is brought out of thermal equilibrium. When switching off this field, the nuclear magnetic moment will tend to align against the external field again at a rate that is dependent on the so-called relaxation times. This will produce a change in the magnetic flux and may generate an electrical current through a coil, where the current is proportional to the proton content and the change in intensity is proportional to the relaxation times.[26−30] This feature is applied to monitor the characteristics, such as relaxation times, bulk, and solid fractions of the sample as the temperature is varied.

2.2. Carr−Purcell−Meiboom−Gill (CPMG) Experiment. To monitor the characteristics of the sample mentioned above, we use the Carr−Purcell−Meiboom−Gill (CPMG) NMR experiment.[30,31] This experiment consists of an initial oscillating magnetic field pulse, radio frequency (RF), which brings the net nuclear magnetic moment 90° away from the direction of the external field (i.e., in the transverse plane to the external field). Then a loop of 180° RF pulses are applied, separated by a time $2 \times \tau$, and the induced current (the NMR signal) is recorded at the time of the spin echoes[32] (Figure S1, Supporting Information). This NMR signal, I, will decay as a function of the transverse relaxation time T_2 and with the corresponding fraction as follows:

$$I = \sum_i I_i e^{-2n\tau/T_2^i} \tag{1}$$

where I is the component number, T_2^i the relaxation time of the component, I_i the corresponding intensity, τ half of the interecho spacing, and n the echo number.[30,31] The experimental data which, in general, has a multiexponential decay can then be fitted to an inverse Laplace transform[32] and will result in a distribution of T_2 values and with their corresponding intensities.

T_1 and T_2 values of molecules are therefore influenced by variations of the NMR interactions due to molecular motion. As a result, T_1 and T_2 measurements have become common approaches to study molecular characteristics such as reorientation of molecules and interaction between them.[27] In this study, T_2 distributions, acquired by CPMG are used to characterize wax crystallization and the mobility of dissolved wax molecules with temperature. Liquids display higher T_2 ranges, conventionally set at above 3×10^{-3} s, while solids are characterized by low T_2 values (10^{-4} to 10^{-3} s).

3. EXPERIMENTAL SECTION

3.1. Materials. Solvents used in this study are deuterated toluene (anhydrous, 99.6% deuterated), toluene (anhydrous, 99.8%), and hexadecane (anhydrous, 99%) from Sigma-Aldrich, Norway. Macrocrystalline wax was provided by Sasolwax from Sasol, Germany (wax 5405). The composition and properties of this wax sample are presented previously.[19] Asphaltenes were precipitated from a heavy crude oil (API 19°) originating from the Norwegian shelf of the

https://doi.org/10.1021/acs.energyfuels.1c03613
Energy Fuels 2022, 36, 350−360

North Sea, using *n*-hexane (HPLC grade, ≥97%). Properties of the asphaltenes precipitated from this crude oil have previously been published.[33,34] The pour point depressant used in this study was based on polycarboxylate (proprietary) from BASF, Germany, and was presented as PPD A previously.[19] As a reference, all concentrations presented in this study are in weight percentages (% wt).

3.2. Sample Preparation. For asphaltene preparation, the selected crude oil was heated to 60 °C for 1 h and shaken strongly before use to ensure homogeneity of the sample. Asphaltenes were precipitated by diluting the crude oil sample with 40 mL *n*-hexane per gram of crude oil and stirring overnight. The resulting mixture was then filtered through a 0.45 μm HVLP-type Millipore filter membrane and afterward rinsed with warm *n*-hexane until the filtrate was clear. The yield of asphaltenes accounted for 2.3%−2.7% of the crude oil.

The PPD originally contained different petroleum cuts having 80% active content, according to manufacturer specifications. The polymers were solvent purified, according to the procedure detailed previously.[19]

In order to prepare the samples used for CPMG NMR analysis, PPDs and asphaltenes were first dissolved in deuterated toluene, obtaining stock solutions with concentrations of 1.05 wt %. These were shaken overnight at 200 rpm to allow for an optimal degree of solubilization. Then, a range of wax−PPD and wax−asphaltene solutions were obtained by dilution of the initial PPD and asphaltene solutions if needed and then by addition of the desired macrocrystalline wax content. A range of wax-only solutions were also prepared by dissolution of wax in deuterated toluene. All wax-containing systems were heated at 60 °C for 1 h and shaken thoroughly. Lastly, 3 g of each solution were introduced into a NMR tube. The solubility of asphaltenes at high concentration (2%) in the wax−asphaltene system was further confirmed with an optical microscope. Two independent parallel experiments were performed with NMR for each system in order to ensure reproducibility. The overall error was calculated from the difference in results obtained with the two parallel experiments and is displayed in the corresponding figures presented in this study.

3.3. Nuclear Magnetic Resonance: CPMG Analysis. NMR experiments were conducted on a low field (21 MHz) NMR spectrometer, which was supplied by Anvendt Teknologi AS, Norway. A CPMG sequence was used to acquire T_2 distributions.[31] In this study, two types of experiments were employed: dynamic experiments, involving a temperature decrease between the measurement points, and some static experiments at constant temperature, described in the Supporting Information.

For the dynamic experiments, the interecho spacing was selected for two regions: a first region with τ_1 of 200 μs and with 6000 echoes, focusing with higher detail on the more sensitive low T_2 area and a second region with τ_2 of 600 μs and with 2000 echoes. T_2 distributions were generated from the multiexponentially decaying curve, using the one-dimensional inverse Laplace transform.[32] They represented a qualitative form of system comparison through the use of 3D contour maps but also a quantitative measure by tracking the intensity of T_2 with temperature in selected regions. Several algorithms in Matlab 2021b were used to further process data and separate signal intensities in different T_2 areas.

In this study, ramping by a rate of 0.2 °C/min was conducted for the dynamic experiments to allow for the system to stabilize during the NMR scan. Stepwise scanning was used from 45 to 0 °C, leaving the system at constant temperature while the measurement at each temperature point was acquired. Selecting the number of scans was performed after some initial trials. A higher number of scans generates a higher amount of time needed for a measurement point at a temperature step and thus a lower number of steps in the temperature ramping. However, in order to have a more detailed temperature history, more temperature steps inside the same time interval are needed, so that the evolution of the system with temperature can be followed with higher resolution. Therefore, although a higher number of scans provide more accurate T_2 results due to the consolidation of the NMR signal, the history-dependent evolution of T_2 is less accurate. First, the number of scans was set at a conventional value of 16, which allowed 68 temperature steps in the 45−0 °C interval. Nevertheless, the number of scans was increased to 32 for experiments where the advantages generated by improvements to the noise reduction and resonance frequency were found to significantly overcome the drawbacks generated by reducing the resolution of the history-dependent scanning. Here, 42 measurement points were achieved in this case in order to ensure the same cooling rate as before. Data were later normalized for these systems to be able to compare the results.

The temperature inside the NMR was controlled with an air flow. First, the air was cooled below room temperature using a water bath with a 60:40 diethylene glycol/water mixture. Then, as it passed through the NMR, the air flow was heated using a high precision thermal controller supplied by Anvendt Teknologi AS. First, a calibration with hexadecane was performed to find the temperature correction needed to account for the inefficiency in thermal exchange between air and the sample in the NMR instrument. Hexadecane dissolved in deuterated toluene (5%) is liquid in the desired temperature range (45−0 °C) and shows a strong signal from the hydrogen atoms. The signal was first acquired dynamically with the desired thermal ramping (0.2 °C/min), and then, static experiments were performed at five constant temperatures inside this interval. As one can observe in Figure S2 in the Supporting Information, the thermal correction needed in our study is negligible, as the gap between the dynamic and the static calibrations is marginal. The dynamic calibration with hexadecane also allows one to correct for signal variation with temperature generated by the different repartitions of hydrogen atoms at different energy levels and quantified by the Boltzmann factor.[30] Thus, the net intensity of the wax signal at each temperature, W_T, is divided by the intensity of hexadecane signal at the corresponding temperature, H_T, and thus, normalized wax signals at each temperature, $W_{\mathrm{normal},T}$ is obtained (eq 2). Then, a set point, W_{sp}, is created by averaging the resulted values inside the expected WAT-45 °C interval, above the wax appearance temperature (eq 3). The apparent dissolved wax content at a defined temperature, $f_{\mathrm{liquid},T}$ is thus determined by dividing the normalized intensity of the wax at that temperature by the averaged set point (eq 4). The equivalent apparent solid wax content, $f_{\mathrm{solid},T}$ is obtained by deducting $f_{\mathrm{liquid},T}$ from 1 (eq 5).

$$W_{\mathrm{normal},T} = \frac{W_T}{H_T} \tag{2}$$

$$W_{sp} = \overline{W_{\mathrm{normal},T}}\ ,\ WAT \le T \le 45°\mathbf{C} \tag{3}$$

$$f_{\mathrm{liquid},T} = \frac{W_{\mathrm{normal},T}}{W_{\mathrm{sp}}} \tag{4}$$

$$f_{\mathrm{solid},T} = 1 - f_{\mathrm{liquid},T} \tag{5}$$

4. RESULTS AND DISCUSSION

This section focuses on selected wax, wax−asphaltene, and wax−PPD systems in deuterated toluene. The analysis of results for each type of system starts from the qualitative correlation of T_2 with the mobility of molecules, continues with wax precipitation evolution, and ends with a new approach to analyze the interactions between the wax crystals and the dissolved wax through the intensity of T_2 in the reduced mobility dissolved wax region. The impact of wax, asphaltene, and PPD concentration is investigated, using each type of analysis.

4.1. Effect of Wax Concentration on Interactions between Wax Crystals and Dissolved Wax. T_2 patterns of wax precipitation in a system comprising of 5% macrocrystalline wax in deuterated toluene are summarized in Figure 1. At high T_2 (10^{-1} to 10^{-0} s), one can notice a main peak corresponding to the wax dissolved in deuterated toluene.

https://doi.org/10.1021/acs.energyfuels.1c03613
Energy Fuels 2022, 36, 350−360

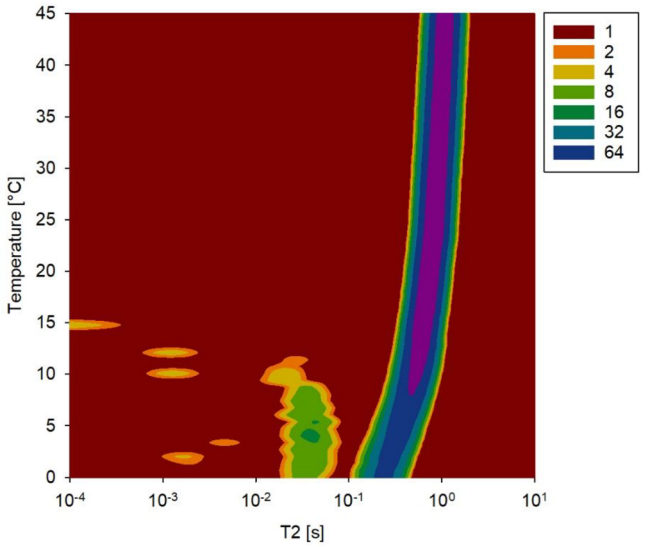

Figure 1. Evolution of T_2 (x-axis) and intensity of T_2 (scatter map) as a function of temperature for 5% wax in deuterated toluene, with no correction for the Boltzmann factor.

From 45 to 20 °C, this peak displays a linear increasing pattern in total intensity from 902 to 1002 a.u. This occurs due to the different repartition of hydrogen atoms at different energy levels generated along the temperature range.[30] The phenomenon is quantified by the Boltzmann factor, which generates linear increases in the intensity of the dissolved wax signal, before wax precipitation starts. Inside this same interval, one can also notice a linear decrease in the T_2 range, generated by an increase of viscosity and an associated reduction of the diffusion coefficient of wax molecules.

As the temperature is reduced further below the wax appearance temperature (≤20 °C), the peak has lower intensity and shifts more abruptly toward lower T_2 values. This is due to wax precipitation. At low T_2, a secondary peak is observed at temperatures below 10 °C. The T_2 of this peak (10^{-3} to 10^{-1} s) corresponds to a region between the liquid phase and phase change to a solid. This region was first qualitatively observed by Ruwoldt et al.,[19] but their method did not allow its quantification.

There are several hypotheses explaining this peak. The decrease in T_2 for a fraction of the dissolved wax molecules corresponds to a decrease in their molecular mobility. The most likely cause for this variation is the fact that molecular mobility decreases when spatial hindrances are imposed on dissolved wax molecules, trapped within the newly formed wax crystal network.[35] The NMR instrument tracks the hydrogen signal of the wax molecules. Thus, the intensity of the secondary peak is directly proportional to the amount of dissolved wax molecules with decreased mobility. The intensity of the peak allows one to quantitatively observe the effect of spatial hindrances imposed on dissolved wax molecules. Consequently, this reflects the amount of interactions between dissolved wax molecules and the wax crystal network. Therefore, the analysis of interactions between dissolved wax molecules and the wax crystal network can be performed qualitatively through the decrease in T_2 and quantitatively through an increase in intensity of the low T_2 region.

Lastly, the precipitated solid wax cannot be observed in the 3D contour map, as the NMR instrument does not record signals at T_2 values characteristic to solids, below 10^{-3}, when measured using a CPMG sequence.

Two more systems, 10% wax in deuterated toluene and 15% wax in deuterated toluene, are investigated with this method to analyze the effect of concentration on wax precipitation and interactions. The 3D contour maps obtained for these systems are presented in Figure S3 and S4 in the Supporting Information. The quality of the measurement is validated through the quasilinear intensification of the main peak with temperature observed above the wax appearance temperature; the intensity is confirmed to be 2.04−2.12 as high for 10% wax than for 5% wax and 3.08−3.20 times as high for 15% wax than for 5% wax. Moreover, similar patterns in the 3D contour maps are observed for the 10% and 15% systems, below the wax appearance temperature: a decrease in T_2 and intensity of T_2, along with the formation of a secondary peak corresponding to reduced mobility dissolved wax.

Wax precipitation curves are determined using eqs 2−5 (i.e., by integrating the signal of the dissolved wax in the main peak at $T_2 = 10^{-1}$ to 10^{0} s, without considering the intensity of the secondary peak). Figure 2 demonstrates a relationship between

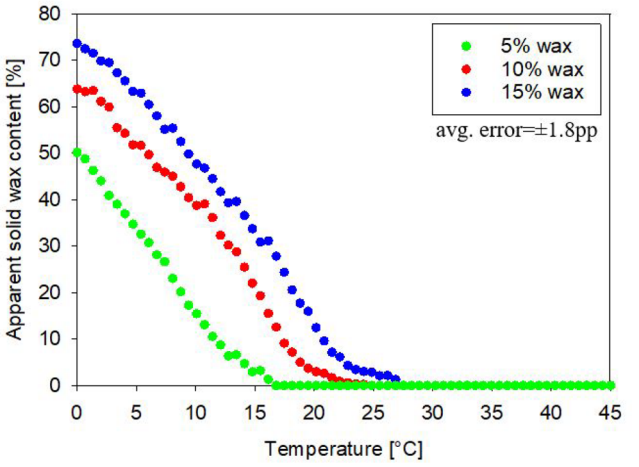

Figure 2. Apparent percentage of precipitated wax as a function of temperature for macrocrystalline wax systems.

the wax precipitation onset temperature and the concentration of wax in solution; the higher the wax concentration is, the higher the wax appearance temperature is. Thus, one can observe that there is a 4−6 °C delay between the points at which precipitation reaches the same level in the 5% wax system and the 10% wax system. A similar 4−6 °C delay is noticed between the corresponding points in the 10% wax system and 15% wax system. For example, the apparent wax solid content reaches 50% at approximately 0 °C for 5% wax, at approximately 5 °C for 10% wax, and at approximately 10 °C for 15% wax.

The novelty with this NMR method is a significant increase in resolution of the reduced mobility dissolved wax peak. This facilitates the analysis of the interactions in the wax crystal network. The approach in this study focuses on quantifying the total secondary peak intensity evolution, as illustrated in Figure 3. This value becomes a parameter which can be correlated to the total amount of dissolved wax molecules whose mobility is reduced by interactions with the new crystals; the more dissolved wax molecules become trapped within the wax crystal network, the stronger in intensity the low mobility dissolved

https://doi.org/10.1021/acs.energyfuels.1c03613
Energy Fuels 2022, 36, 350−360

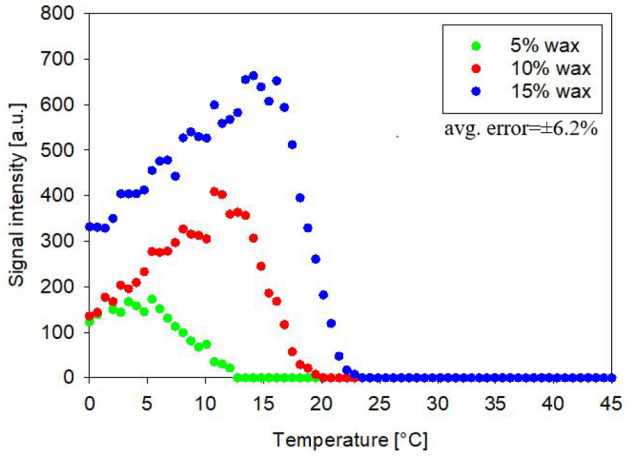

Figure 3. Evolution of total secondary peak intensity as a function of temperature for macrocrystalline wax systems.

wax region is. The secondary peak intensity has a quasisymmetric profile which shows maximums at 18, 12, and 5 °C for 15%, 10%, and 5% wax. More and more dissolved wax has reduced mobility as temperature decreases until the maximum secondary peak intensity is reached. After that point, the amount of reduced mobility dissolved wax molecules progressively decreases. There are two main factors contributing to the total secondary peak intensity. The first factor is the crystallization of dissolved wax molecules trapped in the wax crystal network, which generates further decreases in T_2, shifting their signals to values specific to the solid phase, below the measured range ($<10^{-3}$ s). The second factor is the rate at which molecules at high T_2 become trapped themselves in the wax crystal network to replace the low mobility molecules that are already crystallized. Until the maximum is reached, the rate at which molecules become trapped is higher than the rate of crystallization from the reduced mobility region. After the maximum is reached, the opposite happens. The reason is the fact that at the maximum, precipitation has already been going for a significant time, and the amount of dissolved wax molecules at high T_2 available to become trapped significantly decreases, as one can observe in the wax precipitation curve in Figure 2.

One can also notice a quasilinear trend between the temperature of the secondary peak maximum and the wax concentration. The average total intensity of the dissolved wax trapped in the wax crystal network above 0 °C also shows an increase with wax concentration (114.5, 229.2, and 426.5 a.u. for 5%, 10%, and 15%, respectively). The last two observations demonstrate that the higher the wax concentration in solution is, the more dissolved wax molecules become trapped in the newly formed wax crystal network, and the higher the temperature at which the maximum signal from these complexes occurs. Therefore, one can conclude that inside the analyzed concentration range, wax precipitation and the intensity of the corresponding reduction in mobility of dissolved wax follow a similar pattern, dependent on concentration.

4.2. Characterization of Wax–Asphaltene Interactions. *4.2.1. Behavior of Asphaltenes with Temperature.* The behavior of asphaltenes in the selected temperature range is investigated by using a model asphaltene–hexadecane system. The signal of asphaltenes alone is not enough for the NMR instrument to find the resonance frequency, and therefore, an inert hydrogenated solvent (hexadecane), which does not interact with asphaltenes and does not precipitate, has been added. The analysis of asphaltene behavior is essential to identify the differences between the asphaltene–hexadecane and asphaltene–wax systems presented in the next section. Subsequently, the role of asphaltenes in the observed wax crystals–dissolved wax interactions can be assessed.

Figure 4 emphasizes two reference systems, 5% hexadecane and 5% hexadecane with 1% asphaltenes, both in deuterated toluene. The results illustrate the high T_2, liquid hexadecane peak at $T_2 = 10^{-1}$ to 10^{0} s in both reference systems. However, when asphaltenes are added, an additional low T_2 peak can be observed close to the liquid–solid phase change region (10^{-3}

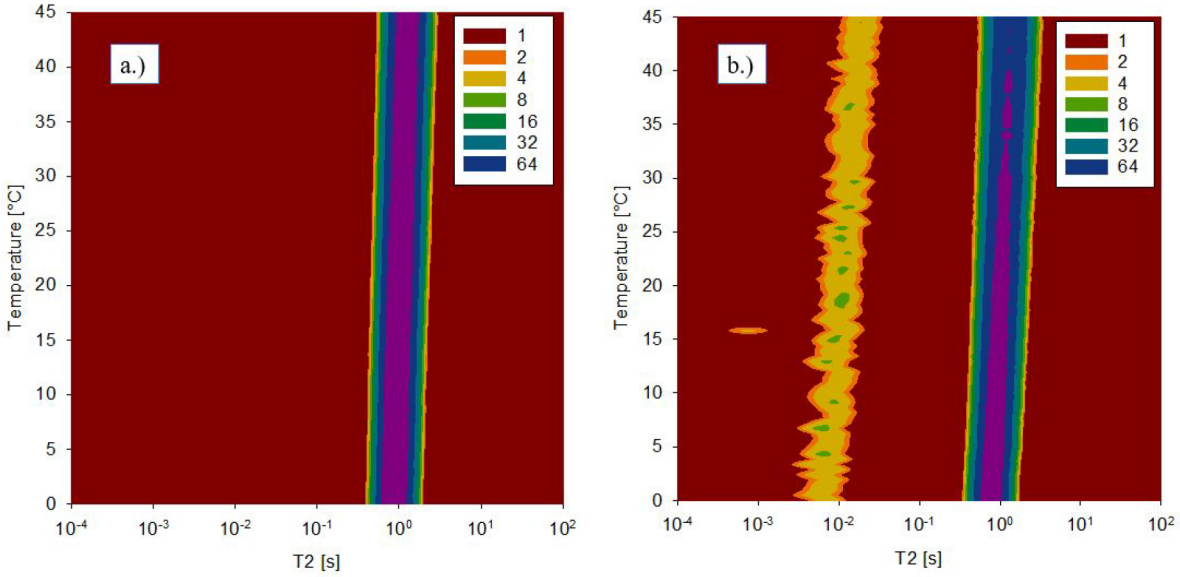

Figure 4. Evolution of T_2 (*x*-axis) and of intensity of T_2 (scatter map) with temperature for (a) 5% hexadecane in deuterated toluene and (b) 5% hexadecane, 1% asphaltene in deuterated toluene, with no correction for the Boltzmann factor.

https://doi.org/10.1021/acs.energyfuels.1c03613
Energy Fuels 2022, 36, 350–360

to 10^{-2} s). This most likely corresponds to asphaltene nanoaggregates in the system.

Asphaltenes are expected to coexist in the system both in dissolved monomer form at high T_2 (in the same region as hexadecane) and in nanoaggregate form at low T_2.[13] The influence of the asphaltenes on the main hexadecane peak was investigated to quantify the part of the peak that does not correspond to hexadecane. Example results at 45 °C show that the intensity of the main peak in the hexadecane system is 961 ± 1.2% a.u., while for the hexadecane/asphaltene system the corresponding intensity is 1019 ± 0.5% a.u. A first assumption would be that the difference of 58 a.u. (5.6%) between the averaged intensities corresponds to liquid asphaltene monomers having a similar T_2 as hexadecane. Over the entire temperature range, there is a 3.5%−7.2% increase in the average main peak intensity in the system with asphaltenes. However, the increase attributed to monomers is partially converging to the uncertainty in the intensity values, generated by noise in the NMR system. This varies in the 0.4%−5.7% interval over the temperature range. Therefore, the monomers will be considered negligible in this study, inside the NMR noise range. The exact quantification of monomers over the entire temperature range remains to be analyzed in the future with a higher precision method.

4.2.2. Effect of Asphaltene Concentration on Interactions between the Crystal Network and Dissolved Wax. To quantify the effect of asphaltene concentration on the dissolved molecules−wax crystals interactions, four systems with the same content of wax (5%) and varying contents of asphaltenes (0.5%, 0.75%, 1%, 2%) were selected. The 0.5% and 0.75% asphaltene systems were scanned using a double number of scans (NS = 32, instead of NS = 16) to overcome the NMR resonance frequency and noise limitations, triggered by low asphaltene concentration and consequently low asphaltene signal, as explained in Section 3.3. Therefore, the intensity values displayed for these systems in the Supporting Information in Figures S5 and S6 are normalized in Figure 7 from NS = 32 to NS = 16 to be able to perform a comparison with the other systems. The 3D contour map for the 2% asphaltene, 5% wax system is also presented in the Supporting Information in Figure S7.

Figure 5 presents the qualitative impact of the addition of 1% asphaltenes to the 5% wax system. When asphaltenes are added, one can observe the expected peak corresponding to wax dissolved in liquid at high T_2 values. At short T_2, above the wax appearance temperature, asphaltene nanoaggregates appear at $T_2 = 10^{-3}$ to 10^{-2} s. The T_2 range of this peak corresponds to the secondary peak observed in Figure 4, and the average intensity above 25 °C is comparable (50.7 a.u. for Figure 5; 47.2 a.u. for Figure 4), with an error inside the noise range of the NMR instrument (≤5%). Once wax precipitation starts, below the wax appearance temperature, the asphaltene nanoaggregate peak present in Figure 5 disappears (only some negligible traces are observed). A new secondary peak with significantly higher intensity is progressively generated at slightly higher T_2 (10^{-2} to 10^{-1} s) by the dissolved wax molecules whose mobility decrease due to interaction with the newly formed crystal network. This peak corresponds to the secondary peak observed in the wax-only system in Figure 1, being recorded in a similar T_2 range (10^{-2} to 10^{-1} s). However, it is generated at a higher temperature and has a higher intensity in the system with asphaltenes. The secondary peak evolution leads to some possible suggestions. The first is

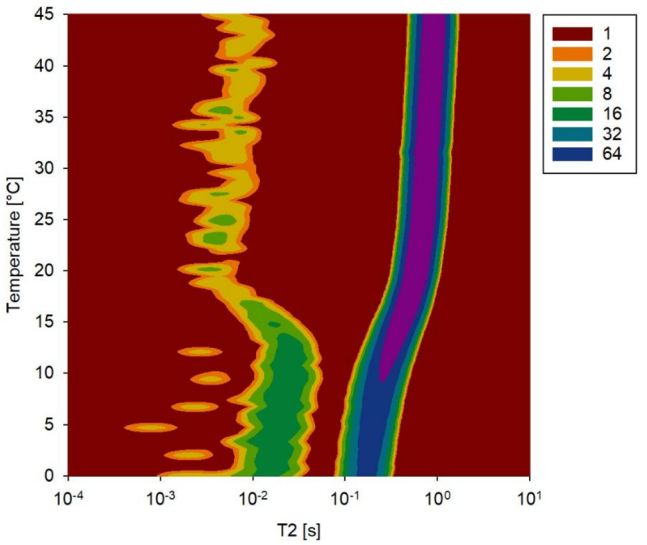

Figure 5. Evolution of T_2 (*x*-axis) and intensity of T_2 (scatter map) with temperature for 5% wax, 1% asphaltene in deuterated toluene − no correction for the Boltzmann factor

that more wax liquid molecules become trapped in the newly formed crystal network with 1% asphaltene than in the system presented in Figure 1 without 1% asphaltene. The second suggestion is that cocrystallization of wax and asphaltenes is the cause for stronger spatial hindrance and thus stronger interactions between the newly formed solid particles and dissolved wax. However, the cocrystallization hypothesis needs to be tested in the future using high resolution NMR for higher accuracy.

A possible physical explanation for the disappearance of the asphaltene nanoaggregate peak is a decrease of the asphaltene nanoaggregate size once wax starts precipitating that would generate an increase in the mobility of asphaltene molecules. This is, however, not likely. A more likely explanation is that cocrystallization of wax and asphaltene occurs, decreasing the T_2 of asphaltenes outside the measured range to solid-specific T_2. The potential cocrystallization behavior has been reported in several publications.[9,15,36] Another explanation for the disappearance of the peak might be the impossibility to separate the NMR signal of the peak corresponding to decreased mobility dissolved wax and of the nanoaggregate peak once wax starts precipitating. However, Figure 7 demonstrates that the increase in secondary peak intensity from above to below WAT for the 5% wax, 1% asphaltene system is higher than the intensity of the secondary peak of 5% wax system. Therefore, the impossibility to separate the peaks due to instrument limitations could only be partially associated with the secondary peak evolution.

Wax precipitation curves in Figure 6 display a significant increase in crystallization rate when 0.75%, 1%, or 2% asphaltenes are added. When the concentration of asphaltenes is 0.5%, one can notice an insignificant effect on wax precipitation. Slight inhibition tendencies below C.A.C. (critical asphaltene concentration) in the 0.05%−0.3% concentration range have also been confirmed in previous studies.[13] Thus, there is a change from little or no effect to wax precipitation promotion from 0.5% to 0.75% for the analyzed type of asphaltenes. Another observation is the shift in precipitation patterns between the four analyzed systems. Crystallization rates and onsets do not vary regularly in the

https://doi.org/10.1021/acs.energyfuels.1c03613
Energy Fuels 2022, 36, 350−360

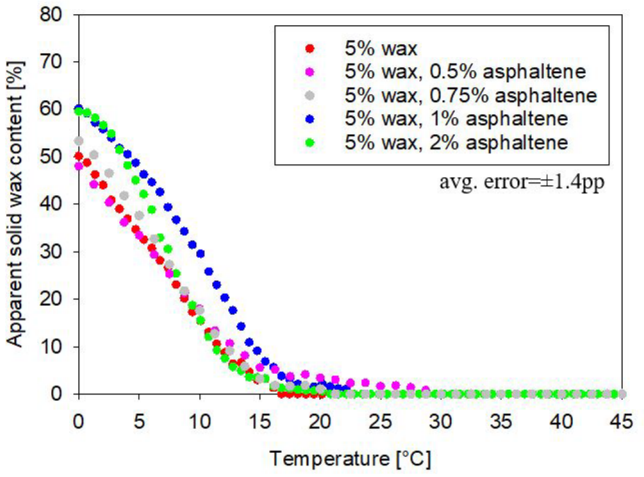

Figure 6. Apparent percentage of precipitated wax as a function of temperature for wax−asphaltene systems.

selected intervals. For example, although the system with 2% asphaltene reaches the highest crystallization rate, recorded in the 5−15 °C interval, its onset is way slower than for the 1% asphaltene system.

An important correction to consider is the part of the main peak at high T_2 caused by the presence of asphaltene monomers, as discussed in Section 4.2.1. If these monomers are deducted in eq 2 from the dissolved wax signal, the calculated solid wax content will increase from the value not accounting for asphaltene monomers, presented in Figure 6. By extrapolating from rough estimations presented in Section 4.2.1, one can expect an upward correction of 3.5%−7.2% for 1% asphaltene system. As a result, the addition of high concentration (≥0.75%) asphaltene most likely leads to crystallization rates, which are higher than the ones presented in Figure 6 by the corresponding correction percentages. However, these values need to be updated with a higher resolution NMR method for higher accuracy, as explained in Section 4.2.1.

Overall, the wax precipitation patterns presented in Figure 6 have links to developments in the literature, which track asphaltene behavior in relation to the critical asphaltene concentration (C.A.C.). This concentration corresponds to the value at which asphaltenes start forming nanoaggregates.[37,38] It is generally considered that above this value the nanoaggregate state of asphaltenes is dominant, whereas below this value, approximately all asphaltenes are in monomer state. Lei and coworkers showed in their study that monomer asphaltenes tend to inhibit wax precipitation just below the corresponding critical asphaltene concentration of 0.3%, while asphaltenes present in aggregate state above 0.3% generate an increase in wax precipitation rate as concentration increases.[14,37] This is in agreement with the results of our study and suggests that the corresponding critical asphaltene concentration for the analyzed kind of asphaltenes is close to the 0.5% concentration point.

A previous study by Kriz and Andersen[13] measured the WAT evolution in crude oil with asphaltene concentration by polarized light microscopy, one of the most accurate WAT identification methods. Their study indicates an irregular pattern for WAT with temperature and a very slow insignificant increase in WAT with asphaltene concentration at values above 0.2%. This is consistent with the results presented in Figure 6, which show very close wax crystallization onsets for the 0.5%−2% concentration range. The authors also illustrate that at high concentration there are two main opposing factors affecting wax precipitation. First, there is an influence of the presence of more asphaltene molecules acting as precipitation sites and thus enhancing the wax precipitation. Second, there are spatial hindrances imposed by the asphaltene particles, possibly larger in volume, on the wax molecules, leading to wax inhibition. However, the authors conclude that at high concentration the effect of concentration is prevailing, although high spatial interference is still present. Therefore, as the amount of aggregated asphaltenes present in the system increases for higher concentration, waxes tend to precipitate faster as a result of the dominant effect of the presence of more asphaltenes acting as precipitation sites. This trend can be observed in the wax precipitation patterns of our study, which show higher precipitation rates at higher concentration. However, the nonlinearity and the irregularities of the precipitation rate with concentration demonstrate that other factors affect this phenomenon too (i.e., nonlinear spatial hindrances, surface area of asphaltenes). As mentioned earlier, the literature also shows that the highest level of inhibition occurs in the monomer dominant region, around C.A.C. At that point, asphaltenes are less likely to act as wax precipitation sites, impose enough spatial hindrances, and are also sufficiently dispersed to affect waxes at molecular level.[9,13]

The hypotheses presented above are further emphasized by the analysis of interactions for wax−asphaltene systems through the total secondary peak intensity. The amount of wax is constant in the selected wax−asphaltene systems (5% wax), and therefore, by quantifying the secondary peak, one can observe the relative change in the amount of reduced mobility dissolved wax molecules when asphaltene concentration is modified. Figure 7 presents values normalized by the

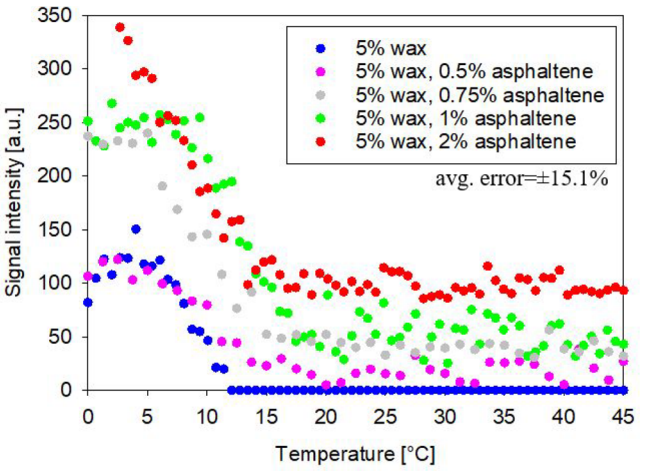

Figure 7. Evolution of total secondary peak intensity with temperature for wax−asphaltene systems, normalized to NS = 16.

number of scans to NS = 16 for the total secondary peak intensity. Above the wax appearance temperature, one can observe the intensity of the asphaltene nanoaggregate peak. The limitation of the NMR system is emphasized by the fact that the lower the concentration of asphaltenes is, the higher the noise in the asphaltene nanoaggregate peak is. However, average values in the 25−45 °C region confirm that for each increase of the asphaltene concentration the secondary peak

https://doi.org/10.1021/acs.energyfuels.1c03613
Energy Fuels 2022, 36, 350−360

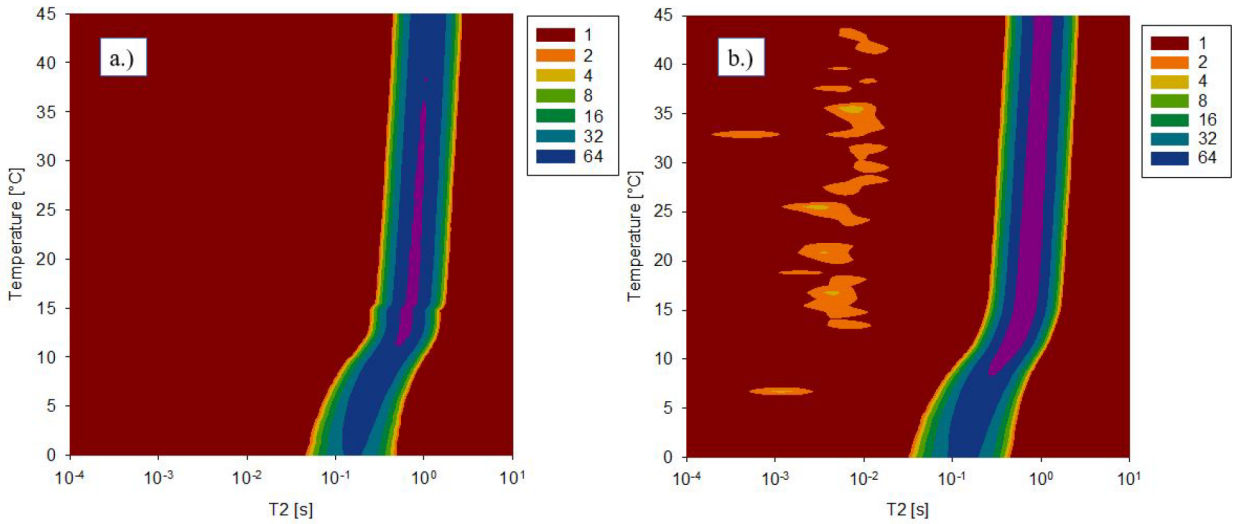

Figure 8. Evolution of T_2 (x-axis) and of intensity of T_2 (scatter map) with temperature for (a) 5% wax, 0.1% PPD in deuterated toluene and (b) 5% wax, 1% PPD in deuterated toluene, before correction for the Boltzmann factor.

intensity increases approximately linearly. This proves the reliability of the method and highlights once again that the secondary peak above WAT at very low T_2 corresponds to asphaltenes. Also, this shows that the percentage of the asphaltenes present in nanoaggregate form is constant above WAT in the analyzed concentration range. On the other hand, below WAT, one can notice an enhancement in the low mobility dissolved wax region for high asphaltene concentrations (0.75%, 1%, and 2%) than for the system without asphaltenes. This demonstrates that when asphaltene concentration is high enough, the signal from wax molecules trapped in the wax−asphaltene crystal network increases significantly with concentration. On the other hand, the system with 0.5% asphaltene shows an insignificant effect on the wax molecules trapped in the crystal network, which can be associated with the same insignificant impact observed in Figure 6 for the wax precipitation rate. This observation can be associated with the results obtained by Ruwoldt et al. with low asphaltene concentration (1000 ppm asphaltene), where a similar trend was noticed.[19]

The results show that a change in asphaltene behavior occurs inside the 0.5%−0.75% interval. One of the potential explanations is a transition in the aggregation state of asphaltenes.[14,39,40] Another explanation is that more, larger asphaltene particles, cocrystallized or "bound" to wax, may be generated at higher asphaltene concentrations, and therefore, they may cause stronger spatial hindrance, generating higher intensity in the corresponding relaxation time region. Consequently, more dissolved wax molecules display a decrease in mobility, as concentration increases. However, the nonlinearity of the pattern can most likely be attributed to the opposing effect of higher asphaltene concentration: higher precipitation rate as a result of more aggregate asphaltene molecules acting as precipitation sites for waxes.

Experiments for systems of 5% wax with and without 1% asphaltenes (Figures S8 and S9, Supporting Information) were carried out at constant temperature (5 and 10 °C) to investigate the evolution of the system over time and to track the intensity of the reduced mobility dissolved wax peak with higher resolution at selected temperatures. Results displayed stability with time and comparable conclusions with the dynamic systems.

Figures S10−S12 of the Supporting Information illustrate the degree of reproducibility of the method for the 5% wax, 1% asphaltene system.

4.3. Effect of PPD Addition on Wax Precipitation.

Figure 8 qualitatively presents the effect of PPD addition on wax crystallization. A first observation is that the main peak at high T_2 now broadens more at low temperature than for wax−asphaltenes (Figure 5) or only wax (Figure 1), indicating that dissolved waxes in the main peak have a wider distribution of the mobility range when the PPD is added. Both dissolved wax and dissolved PPD molecules interacting with wax are expected to be present in the high T_2 peak. At low T_2, above the wax appearance temperature, a secondary peak is noticed in the high concentration PPD system (1%). Below the wax appearance temperature, there is no visible peak at short T_2 for both concentrations. The explanation is that a proportion of PPD molecules most likely modify dissolved wax behavior by liquid complex formation and fast cocrystallization, preventing dissolved wax molecules from being trapped in a higher viscosity crystal network, like in wax and wax−asphaltene systems. The secondary peak that we observe for the 1% system at temperatures higher than 15 °C can thus be associated with PPD macromolecules, displaying weak constant intensity in the 45−15 °C interval. However, below 15 °C, when wax precipitation is ongoing at a fast rate, this peak starts to disappear, most likely due to PPD crystallization with wax, which shifts the PPD signal outside the analyzed the T_2 range (in solid state). The presence of the secondary peak in the PPD−wax system is compared with the presence of a similar peak in a reference PPD−hexadecane system in the entire 45−0 °C range. The 3D contour map for this reference system is presented in the Supporting Information in Figure S13. Moreover, the effect of the PPD addition on the main hexadecane peak is insignificant, generating an increase within 5%, which is assumed to be either due to the noise of the NMR instrument or due to dissolved PPD molecules being involved in complex formation with dissolved waxes even above the wax appearance temperature. Therefore, the PPD influence on the main peak

https://doi.org/10.1021/acs.energyfuels.1c03613
Energy Fuels 2022, 36, 350−360

is considered marginal for the generation of the wax precipitation curve.

The secondary peak at high temperature is not observed in the system with 0.1% PPD in Figure 8a. The reason is the inability of the NMR instrument to detect very low signals, corresponding to 10 times less than at 1% PPD, which already has a very low PPD signal at low T_2.

This behavior is comparable to recent advances in PPD studies, which emphasize the cocrystallization of wax and PPD molecules.[7] Moreover, the literature reviews the active role of the incorporated PPD molecule on imposing steric hindrances to wax molecules that further precipitate on the crystal, a process which is achieved through polar moieties in the polymer molecules. This may explain the broadening in the mobility range of dissolved wax molecules at low temperature when more PPD is added. The wax−PPD complexes, however, unlike wax−wax and wax−asphaltene complexes, are more likely to be in high T_2 liquid form and then to directly crystallize. They do not seem to cause persistent significant reductions in dissolved wax mobility as a transition state toward the solid phase.

Additionally, by analyzing wax precipitation curves in Figure 9, one can notice a substantial decrease in wax precipitation

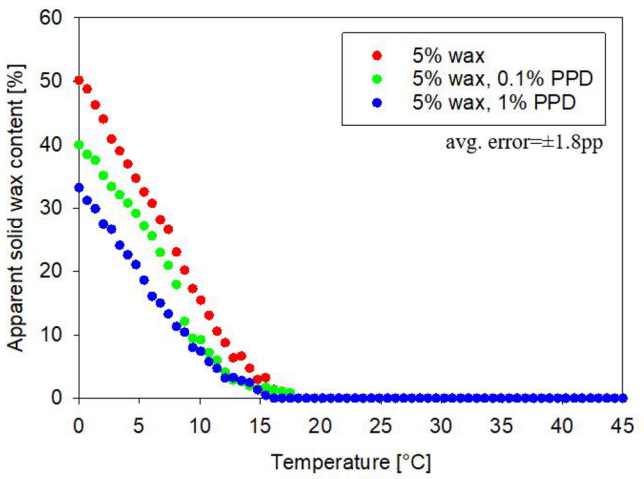

Figure 9. Apparent percentage of precipitated wax as a function of temperature for wax−PPD systems.

rates, which is stronger for higher concentrations. This demonstrates the wax inhibition effect of the PPD and emphasizes the fact that the broadening of T_2 and slight shift to lower T_2 in the main peak may also be attributed to more liquid complexes between the dissolved wax molecules and the inhibitor present at low temperatures than for the other analyzed systems. This consequently also links to developments in the literature which illustrate that PPD polymers increase the thermodynamic solubility of wax through the formation of liquid complexes.[41] Overall, the inhibitor behavior is comparable with other studies about PPD effects on wax precipitation.[42−45]

5. CONCLUSION

This study presents a new low field NMR approach for the analysis of paraffin wax precipitation patterns in model systems, along with the qualitative and quantitative characterizations of wax−wax, wax−asphaltenes, and wax−PPD interactions with temperature through the measurements of relaxation times and their intensities. This method represents an addition to the more established techniques (CPM, DSC) of characterizing wax precipitation patterns and allows a higher resolution NMR characterization of the effects of interactions which influence the wax precipitation mechanism in wax, wax−asphaltenes, and wax−PPD systems.

The main conclusions of this study are summarized below:

(a) In wax-only systems, the T_2 distributions indicate the formation of an intermediate low mobility liquid region, corresponding to dissolved wax molecules on which spatial hindrances are imposed by the newly formed wax crystals. Interactions between dissolved wax and the wax crystal network were previously indicated as a factor influencing wax crystallization. However, this method now allows one to quantify the amount of dissolved wax molecules with reduced mobility generated by trapping inside the wax crystal network as a result of spatial hindrance.

(b) In wax−asphaltene systems, asphaltene nanoaggregates were recorded at low relaxation times above the wax appearance temperature. As wax starts crystallizing, this peak disappears, and an area of reduced mobility dissolved wax is again developed. In this case, the intensity of the dissolved wax molecules with reduced mobility is significantly higher than for the wax-only systems with the same wax content, most likely due to higher spatial hindrances imposed by the larger wax−asphaltene cocrystals. The increase in nanoaggregate asphaltene molecules present at high concentration, acting as nucleation sites, promotes wax precipitation. However, there is no linear pattern, most likely due to the secondary, opposite effect of higher asphaltene concentration: higher spatial hindrances on the dissolved wax, which tend to inhibit crystal formation. Asphaltene nanoaggregate identification and relative quantification represent a novelty in LF-NMR oil research. Moreover, this method allows for the first time one to quantify the effect of asphaltene concentration on the mobility of dissolved wax molecules and on wax precipitation rate. The technique might thus be used in the future to the quantify asphaltene monomer/nanoaggregate ratio or even to approximate the range of critical asphaltene concentration by analyzing the effect of asphaltenes on the wax crystallization rate.

(c) In wax−PPD systems, the higher the PPD concentration is, the lower both wax precipitation rate and wax crystallization onset are, as expected. Liquid complexes between wax and PPD and consequent steric hindrances imposed by the incorporated PPD modify the wax crystallization behavior. PPD macromolecules are observed at low T_2 at high PPD concentration, above the wax appearance temperature, but the recorded peak disappears as wax starts precipitating. This qualitative form of validating wax−PPD interactions such as complex formation and cocrystallization represents a novelty in the LF-NMR oil research.

■ ASSOCIATED CONTENT

Supporting Information

The Supporting Information is available free of charge at https://pubs.acs.org/doi/10.1021/acs.energyfuels.1c03613.

https://doi.org/10.1021/acs.energyfuels.1c03613
Energy Fuels 2022, 36, 350−360

Figures presenting the NMR sequence profile; NMR calibration with hexadecane solution; and 3D contour maps for 10% wax, 15% wax, 5% wax with 0.5% asphaltene, 5% wax with 0.75% asphaltene, 5% wax with 2% asphaltene, and 5% hexadecane with 1% PPD (everything in deuterated toluene). Section detailing the work with static experiments for 5% wax, 1% asphaltene in deuterated toluene. (PDF)

AUTHOR INFORMATION

Corresponding Author

George Claudiu Savulescu − *Ugelstad Laboratory, Norwegian University of Science and Technology, 7491 Trondheim, Norway;* orcid.org/0000-0003-3278-0745; Email: george.c.savulescu@ntnu.no

Authors

Sébastien Simon − *Ugelstad Laboratory, Norwegian University of Science and Technology, 7491 Trondheim, Norway;* orcid.org/0000-0002-3101-4267

Geir Sørland − *Ugelstad Laboratory, Norwegian University of Science and Technology, 7491 Trondheim, Norway; Anvendt Teknologi AS, 7022 Trondheim, Norway*

Gisle Øye − *Ugelstad Laboratory, Norwegian University of Science and Technology, 7491 Trondheim, Norway*

Complete contact information is available at: https://pubs.acs.org/10.1021/acs.energyfuels.1c03613

Notes

The authors declare no competing financial interest.

ACKNOWLEDGMENTS

This work is part of SUBPRO SFI, a research-based center within subsea production and processing. The authors hereby acknowledge the financial support from SUBPRO, which is financed by the Research Council of Norway, major industry partners, and NTNU. Moreover, we hereby acknowledge Dr. Jost Ruwoldt for insightful conversations regarding sample preparation and method background.

REFERENCES

(1) Oliveira, L. M.S.L.; Nunes, R. C.P.; Melo, I. C.; Ribeiro, Y. L.L.; Reis, L. G.; Dias, J. C.M.; Guimaraes, R. C.L.; Lucas, E. F. Evaluation of the Correlation between Wax Type and Structure/Behavior of the Pour Point Depressant. *Fuel Process. Technol.* **2016**, *149*, 268−274.

(2) Kelland, M. *Production Chemicals for the Oil and Gas Industry*; CRC Press, 2009. DOI: 10.1201/9781420092974.

(3) Paso, K.; Senra, M.; Yi, Y.; Sastry, A. M.; Fogler, H. S. Paraffin Polydispersity Facilitates Mechanical Gelation. *Ind. Eng. Chem. Res.* **2005**, *44* (18), 7242−7254.

(4) Venkatesan, R.; Nagarajan, N.; Paso, K.; Yi, Y.-B.; Sastry, A.; Fogler, H. S. The Strength of Paraffin Gels Formed under Static and Flow Conditions. *Chem. Eng. Sci.* **2005**, *60*, 3587−3598.

(5) Yang, F.; Zhao, Y.; Sjöblom, J.; Li, C.; Paso, K. Polymeric Wax Inhibitors and Pour Point Depressants for Waxy Crude Oils: A Critical Review. *J. Dispersion Sci. Technol.* **2015**, *36*, 213−225.

(6) Al-Yaari, M. Paraffin Wax Deposition: Mitigation and Removal Techniques. In *SPE Saudi Arabia Section Young Professionals Technical Symposium*, Dhahran, Saudi Arabia, March 2011; SPE-155412-MS. DOI: 10.2118/155412-MS.

(7) Wei, B. Recent Advances on Mitigating Wax Problem Using Polymeric Wax Crystal Modifier. *J. Pet. Explor. Prod. Technol.* **2015**, *5* (4), 391−401.

(8) Bai, Y.; Bai, Q. Wax and Asphaltenes. In. *Subsea Engineering Handbook*, Second ed.; Bai, Y., Bai, Q., Eds.; Gulf Professional Publishing: Boston, **2019**; pp 435−453. .

(9) Venkatesan, R.; Östlund, J.-A.; Chawla, H.; Wattana, P.; Nydén, M.; Fogler, H. S. The Effect of Asphaltenes on the Gelation of Waxy Oils. *Energy Fuels* **2003**, *17* (6), 1630−1640.

(10) Oliveira, G. E.; Mansur, C. R. E.; Lucas, E. F.; González, G.; de Souza, W. F. The Effect of Asphaltenes, Naphthenic Acids, and Polymeric Inhibitors on the Pour Point of Paraffins Solutions. *J. Dispersion Sci. Technol.* **2007**, *28* (3), 349−356.

(11) García, M. del C. Crude Oil Wax Crystallization. The Effect of Heavy n-Paraffins and Flocculated Asphaltenes. *Energy Fuels* **2000**, *14* (5), 1043−1048.

(12) Molina, V. D.; Ariza León, E.; Chaves-Guerrero, A. Understanding the Effect of Chemical Structure of Asphaltenes on Wax Crystallization of Crude Oils from Colorado Oil Field. *Energy Fuels* **2017**, *31* (9), 8997−9005.

(13) Kriz, P.; Andersen, S. I. Effect of Asphaltenes on Crude Oil Wax Crystallization. *Energy Fuels* **2005**, *19* (3), 948−953.

(14) Lei, Y.; Han, S.; Zhang, J. Effect of the Dispersion Degree of Asphaltene on Wax Deposition in Crude Oil under Static Conditions. *Fuel Process. Technol.* **2016**, *146*, 20−28.

(15) Ariza Leon, E.; Molina Velasco, D. R.; Chavez Guerrero, A. Review of Studies on Asphaltene-Wax Interaction and the Effect Thereof on Crystallization. *Ciencia, Tecnología y Futuro* **2014**, *5*, 39−54.

(16) Kurniawan, M.; Subramanian, S.; Norrman, J.; Paso, K. Influence of Microcrystalline Wax on the Properties of Model Wax-Oil Gels. *Energy Fuels* **2018**, *32* (5), 5857−5867.

(17) Ruwoldt, J.; Kurniawan, M.; Oschmann, H.-J. Non-Linear Dependency of Wax Appearance Temperature on Cooling Rate. *J. Pet. Sci. Eng.* **2018**, *165*, 114−126.

(18) Ruwoldt, J.; Simon, S.; Norrman, J.; Oschmann, H.-J.; Sjöblom, J. Wax-Inhibitor Interactions Studied by Isothermal Titration Calorimetry and Effect of Wax Inhibitor on Wax Crystallization. *Energy Fuels* **2017**, *31* (7), 6838−6847.

(19) Ruwoldt, J.; Humborstad Sørland, G.; Simon, S.; Oschmann, H.-J.; Sjöblom, J. Inhibitor-Wax Interactions and PPD Effect on Wax Crystallization: New Approaches for GC/MS and NMR, and Comparison with DSC, CPM, and Rheometry. *J. Pet. Sci. Eng.* **2019**, *177*, 53−68.

(20) Ruwoldt, J.; Kurniawan, M.; Humborstad Sørland, G.; Simon, S.; Sjöblom, J. Influence of Wax Inhibitor Molecular Weight: Fractionation and Effect on Crystallization of Polydisperse Waxes. *J. Dispersion Sci. Technol.* **2020**, *41* (8), 1201−1216.

(21) Zhao, Y.; Paso, K.; Norrman, J.; Ali, H.; Sørland, G.; Sjöblom, J. Utilization of DSC, NIR, and NMR for Wax Appearance Temperature and Chemical Additive Performance Characterization. *J. Therm. Anal. Calorim.* **2015**, *120* (2), 1427−1433.

(22) Batsberg Pedersen, W.; Baltzer Hansen, A.; Larsen, E.; Nielsen, A. B.; Roenningsen, H. P. Wax Precipitation from North Sea Crude Oils. 2. Solid-Phase Content as Function of Temperature Determined by Pulsed NMR. *Energy Fuels* **1991**, *5* (6), 908−913.

(23) Ruffier-Meray, V.; Roussel, J.; Defontaines, A. Use of Pulsed Nmr Spectroscopy to Measure the Amount of Solid Deposits As a Function of Temperature in Waxy Crudes. *Rev. Inst. Fr. Pet.* **1998**, *53*, 531−535.

(24) Kané, M.; Djabourov, M.; Volle, J.-L.; Rutledge, D. N. Correction of Biased Time Domain NMR Estimates of the Solid Content of Partially Crystallized Systems. *Appl. Magn. Reson.* **2002**, *22* (3), 335.

(25) Yalaoui, I.; Chevalier, T.; Levitz, P.; Darbouret, M.; Palermo, T.; Vinay, G.; Barré, L. Probing Multiscale Structure and Dynamics of Waxy Crude Oil by Low-Field NMR, X-Ray Scattering, and Optical Microscopy. *Energy Fuels* **2020**, *34* (10), 12429−12439.

(26) Pradhan, S.; Rajamani, S.; Agrawal, G.; Dash, M.; Samal, S. K. NMR, FT-IR and Raman Characterization of Biomaterials. In *Characterization of Polymeric Biomaterials*; Tanzi, M. C., Farè, S.,

Eds.; Woodhead Publishing, 2017; pp 147−173. DOI: 10.1016/B978-0-08-100737-2.00007-8.
(27) Hornak, J. P.; *Basics of NMR*; Rochester Institute of Technology, Center for Imaging Science, 1996.
(28) Duus, J. Roger S. Macomber. A Complete Introduction to Modern NMR Spectroscopy. Wiley, Chichester, 1998, Xvii+ 383 Pp. Price £45. ISBN 0 471 15736 8. *Magn. Reson. Chem.* **2002**, *40* (6), 430.
(29) Sørland, G. H. *Dynamic Pulsed-Field-Gradient NMR*; Springer Series in Chemical Physics; Springer, 2014.
(30) Slichter, C. P. *Principles of Magnetic Resonance*; Springer Science & Business Media, 2013.
(31) Meiboom, S.; Gill, D. Modified Spin-Echo Method for Measuring Nuclear Relaxation Times. *Rev. Sci. Instrum.* **1958**, *29* (8), 688−691.
(32) Provencher, S. W. A Constrained Regularization Method for Inverting Data Represented by Linear Algebraic or Integral Equations. *Comput. Phys. Commun.* **1982**, *27* (3), 213−227.
(33) Subramanian, S.; Sørland, G. H.; Simon, S.; Xu, Z.; Sjöblom, J. Asphaltene Fractionation Based on Adsorption onto Calcium Carbonate: Part 2. Self-Association and Aggregation Properties. *Colloids Surf., A* **2017**, *514*, 79−90.
(34) Pinto, F. E.; Barros, E. V.; Tose, L. V.; Souza, L. M.; Terra, L. A.; Poppi, R. J.; Vaz, B. G.; Vasconcelos, G.; Subramanian, S.; Simon, W.; et al. Fractionation of Asphaltenes in N-Hexane and on Adsorption onto CaCO3 and Characterization by ESI(+)FT-ICR MS: Part I. *Fuel* **2017**, *210*, 790−802.
(35) Jestin, J.; Barré, L. Application of NMR Solvent Relaxation and SAXS to Asphaltenes Solutions Characterization. *J. Dispersion Sci. Technol.* **2004**, *25*, 341−347.
(36) Alcazar-Vara, L. A.; Garcia-Martinez, J. A.; Buenrostro-Gonzalez, E. Effect of Asphaltenes on Equilibrium and Rheological Properties of Waxy Model Systems. *Fuel* **2012**, *93*, 200.
(37) Lei, Y.; Han, S.; Zhang, J.; Bao, Y.; Yao, Z.; Xu, Y. Study on the Effect of Dispersed and Aggregated Asphaltene on Wax Crystallization, Gelation, and Flow Behavior of Crude Oil. *Energy Fuels* **2014**, *28* (4), 2314−2321.
(38) Mullins, O. C. The Modified Yen Model. *Energy Fuels* **2010**, *24* (4), 2179−2207.
(39) Mullins, O. C.; Sabbah, H.; Eyssautier, J.; Pomerantz, A. E.; Barré, L.; Andrews, A. B.; Ruiz-Morales, Y.; Mostowfi, F.; McFarlane, R.; Goual, L. R. N.; et al. Advances in Asphaltene Science and the Yen−Mullins Model. *Energy Fuels* **2012**, *26* (7), 3986−4003.
(40) Eyssautier, J.; Levitz, P.; Espinat, D.; Jestin, J.; Gummel, J.; Grillo, I.; Barré, L. Insight into Asphaltene Nanoaggregate Structure Inferred by Small Angle Neutron and X-Ray Scattering. *J. Phys. Chem. B* **2011**, *115* (21), 6827−6837.
(41) Claudy, P.; Létoffé, J.-M.; Bonardi, B.; Vassilakis, D.; Damin, B. Interactions between N-Alkanes and Cloud Point-Cold Filter Plugging Point Depressants in a Diesel Fuel. A Thermodynamic Study. *Fuel* **1993**, *72* (6), 821−827.
(42) Wu, Y.; Ni, G.; Yang, F.; Li, C.; Dong, G. Modified Maleic Anhydride Co-Polymers as Pour-Point Depressants and Their Effects on Waxy Crude Oil Rheology. *Energy Fuels* **2012**, *26* (2), 995−1001.
(43) Paso, K. G.; Krückert, K. K.; Oschmann, H.-J.; Ali, H.; Sjöblom, J. PPD Architecture Development via Polymer−Crystal Interaction Assessment. *J. Pet. Sci. Eng.* **2014**, *115*, 38−49.
(44) Jung, T.; Kim, J.-N.; Kang, S.-P. Influence of Polymeric Additives on Paraffin Wax Crystallization in Model Oils. *Korean J. Chem. Eng.* **2016**, *33* (6), 1813−1822.
(45) Pedersen, K. S.; Rønningsen, H. P. Influence of Wax Inhibitors on Wax Appearance Temperature, Pour Point, and Viscosity of Waxy Crude Oils. *Energy Fuels* **2003**, *17* (2), 321−328.

https://doi.org/10.1021/acs.energyfuels.1c03613
Energy Fuels 2022, 36, 350−360